JOURNAL OF GEOPHYSICAL RESEARCH, VOL. 105, NO. C11, PAGES 26,313–26,331, NOVEMBER 15, 2000

A one-dimensional percolation model of flooding and snow ice formation on Antarctic sea ice

Ted Maksym and Martin O. Jeffries

Geophysical Institute, University of Alaska Fairbanks

Abstract. A one-dimensional thermodynamic sea ice growth model is developed with emphasis on seawater flooding and snow ice formation on Antarctic sea ice. To examine the possibility that flooding is the result of brine percolation through a porous ice matrix, and the consequences of this percolation on the salinity structure and mass balance of the ice, flooding is modeled in a semiheuristic fashion by examining two possible regimes for seawater and brine infiltration through the porous ice into the snowpack. A standard model assumes that the upward flow of brine is horizontally homogeneous and brine flow is modeled using a Darcian scheme. A simple model assumes that the infiltrating brine does not interact with the internal ice brine network, but instead percolates upward through cracks, or is restricted in spatial extent. Results of simulations are shown for the climatology in the Ross Sea and compared to field data from one autumn and one winter cruise aboard the R/V *Nathaniel B. Palmer* in 1995. Sensitivity studies are performed to show the effects of variations in climate forcing. The dependence of brine percolation and snow ice formation on key thermophysical parameters is investigated. Results indicate that the mass balance depends very strongly on the brine flow regime. In the standard model, ice salinities and brine volumes are greatly affected by brine percolation, creating a strong feedback between flooding and future snow ice production. Snow ice formation for the simple model was much more predictable and depended primarily on snow load. Comparison of results with field data indicate that if brine percolation is the major mechanism for flooding and snow ice formation, then there must be either substantial convective redistribution of salt to maintain ice porosity, or the flow must be spatially inhomogeneous.

1. Introduction

In recent years, increased attention to Antarctic sea ice geophysics has revealed that a number of ice growth processes play important roles in the overall ice mass balance. Congelation ice formation has long been recognized as an important ice growth process, and the importance of frazil ice formation and the "pancake cycle" has been noted as possibly the dominant mechanism for ice growth [*Weeks and Ackley*, 1986; *Lange et al.*, 1990]. More recently, snow ice formation has been recognized as a widespread and important phenomenon in all regions of the Antarctic pack ice [*Eicken et al.*, 1994; *Jeffries and Adolphs*, 1997; *Jeffries et al.*, 1997, 1998a, 1998b; *Lange et al.*, 1989; *Worby et al.*, 1998].

In the Antarctic, where snow accumulation rates over the pack ice are relatively high [*Giovinetto et al.*, 1992], the weight of the overlying snow cover will commonly depress the ice surface below sea level, resulting in a negative freeboard, that is, the height of the ice surface lies below the seawater level. When this occurs, there is the potential for sea water and/or brine to infiltrate into the snow cover, flooding the ice surface and creating a highly saline slushy layer at the base of the snowpack. Under cold atmospheric conditions, this slushy layer may refreeze, leading to the formation of snow ice [e.g., *Leppäranta*, 1983]. As the freezing interface is much closer to the surface than for congelation ice growth, snow ice formation can be a very effective mechanism for thickening. In the Pacific sector of the Southern Ocean, for example, there is ample evidence that snow ice contributes as much as 40% of the total ice mass and is thus as important to thickening the ice cover as congelation ice growth and pancake formation [*Jeffries and Adolphs*, 1997; *Jeffries et al.*, 1997, 1998a, 1998b].

Flooding of the snow/ice interface may occur in a number of ways [*Ackley*, 1986; *Ackley and Sullivan*, 1994; *Massom et al.*, 1997]. Seawater may infiltrate laterally from the edges of floes where they are in contact with the ocean. In and around areas of deformed ice, such as in ridges or near the margins of rafts, the

Paper number 2000JC900130.
0148-0227/00/2000JC900130$09.00.

ice is often poorly consolidated and seawater may readily reach the snowpack through fractures. There may also be cracks through which seawater may seep upwards and spread laterally through the snowpack on undeformed ice. Lastly, brine may percolate vertically through interconnected brine pathways in porous sea ice. While all these mechanisms are likely to occur to some degree, the last is presumed to be the most frequent and most important process, and has been implicitly assumed in other studies [*Crocker and Wadhams*, 1989; *Hudier et al.*, 1995; *Jeffries and Adolphs*, 1997; *Jeffries et al.*, 1998a, 1998b; *Golden et al.*, 1998]. Most investigators have not addressed the physical processes involved in brine percolation beyond noting that for flooding to occur, the sea ice must be permeable [*Eicken et al.*, 1995; *Jeffries et al.*, 1998a, 1998b].

The flooding/snow ice formation process has been the subject of some modeling studies [*Leppäranta*, 1983; *Eicken et al.*, 1995; *Crocker and Wadhams*, 1989; *Fritsen et al.*, 1998]. Early efforts [e.g., *Leppäranta*, 1983] assumed that a negative freeboard was the only requirement for flooding to occur. While this is certainly necessary, it is not the only requirement. There also must be established pathways from the ocean through to the snow/ice interface for seawater and/or brine to flow.

Freeboard data from one autumn and one winter cruise in the Ross Sea [see *Jeffries et al.*, 1998a] illustrate the fact that the snow/ice interface does not flood simply because the ice surface is below sea level (Figure 1). While 37% of the observed freeboards were negative, very few of the drilling sites were observed to be wet or flooded at the base of the snowpack prior to drilling. *Eicken et al.* [1995] noted similar results in the Weddell Sea. Not until freeboards approached -6 cm did we observe a significant number of sites that were flooded prior to drilling. It should be noted that this flooding is not necessarily associated with areas of ice deformation [*Adolphs*, 1998,Figure 8]. Flooding is as likely to occur in areas of level ice where no obvious cracks or pathways for upward brine flow are apparent.

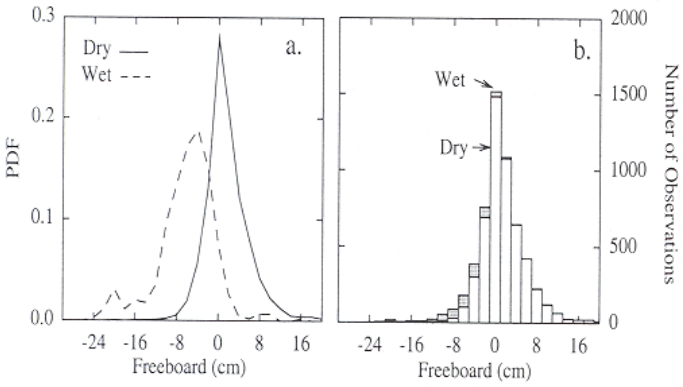

Figure 1. Flooding as a function of freeboard in drill holes in first-year ice in the Ross Sea in autumn and winter 1995. (a) Probability distribution of freeboards for sites that were dry prior to drilling (solid line) and locations that were wet or flooded prior to drilling (dashed line). (b) Frequency distribution of freeboards observed, indicating fraction that were wet or flooded prior to drilling.

Obviously, the presence of a negative freeboard is insufficient to guarantee flooding. *Eicken et al.* [1995], based on unpublished permeability studies, speculated that under certain conditions, even though there is a negative freeboard, the underlying ice might be impermeable and prevent the upward movement of brine to the snow/ice interface. *Cox and Weeks* [1975], in their classic study of desalination processes, demonstrated that artificial sea ice becomes permeable at brine volumes exceeding 5-7%. At lower brine volumes, the brine pockets and channels are not sufficiently connected to allow brine flow. *Golden et al.* [1998], by analogy with electrical conductivity of compressed powders, suggested that the percolation threshold for columnar sea ice occurs for brine volumes of about 5%, and somewhat higher for granular ice. *Eicken et al.* [1995] showed that in the Weddell Sea, brine volumes may be below this threshold throughout much of the growth season.

As the porosity of the ice is closely linked to the thermal regime and the salinity characteristics of the ice, there is a strong coupling between the permeability and the flow regime. While the importance of ice permeability in controlling the flooding process has been noted [*Crocker and Wadhams*, 1989; *Hudier et al.*, 1995; *Lytle and Ackley*, 1996; *Fritsen et al.*, 1998; *Golden et al.*, 1998], little attention has been paid to the complex relationships between flooding, desalination, and ice permeability.

The aims of this study are (1) to investigate whether the percolation model for flooding is a plausible mechanism and whether it produces snow ice amounts similar to those inferred from ice core structural analysis and oxygen isotope data, (2) to identify the critical factors that control the flooding process and their consequences for the overall ice mass balance, and (3) to demonstrate the importance of the coupling between flooding and snow ice formation and the evolution of the salinity characteristics of the ice.

In order to investigate these processes and the factors controlling them, a one-dimensional (1-D), nonlinear sea ice growth model is developed. The evolution of the salinity profile is treated in a semiheuristic fashion and is coupled to ice growth processes and flooding. The sea ice is modeled as a porous medium, and upward brine flow is described using a Darcian scheme. First, the governing equations of the model are presented, and different possible treatments of the brine flow regime are discussed. Model results of ice mass balance and salinity characteristics are presented and compared with field data, and the key parameters controlling ice growth are pointed out. The sensitivity of snow ice formation to several critical parameters is presented, and the importance of factors controlling brine percolation and the salinity profile is discussed. Finally,

we point out gaps in our understanding of the flooding and snow ice formation process.

2. Model Description

A one-dimensional nonlinear ice growth model was developed. The basic model builds on the previous work of *Maykut and Untersteiner* [1971], *Cox and Weeks* [1988] and *Wade* [1993]. The essential framework of the thermodynamics and salinity entrapment and desalination is based on that of *Cox and Weeks* [1975]. However, as we are interested in complex thermophysical interactions between the snow cover and brine network of the ice, the model is extended to allow for nonlinear temperature profiles and for upward brine flow through the ice and snow. As processes related to the snow cover are critical for resolving the phenomena of interest, the snowpack is treated in more detail than in standard sea ice growth models [e.g., *Cox and Weeks*, 1988].

2.1. Thermodynamics

The generalized one-dimensional heat equation for heat transfer in a porous medium is given by

$$\rho_{si,s} C_{si,s} \frac{dT}{dt} + \rho_b C_b \frac{d}{dz}(\phi u T) = \frac{d}{dz}(k_{si,s} \frac{dT}{dz}) + \kappa I_o e^{-\kappa z}, \quad (1)$$

where $\rho_{si,s}$ is the bulk density of sea ice or snow, $C_{si,s}$ is the specific heat, $k_{si,s}$ is the bulk thermal conductivity, ρ_b is the brine density, C_b is the specific heat of the brine, T is the temperature, ϕ is the effective porosity of the bulk medium, and u is the pore fluid velocity. Here, $C_{si,s}$ is an effective specific heat, as it includes the latent heat due to changes in the volume fraction of entrapped brine. *Schwerdtfeger* [1963] gave $C_{si,s}$ as

$$C_{si,s} = -\frac{S}{\beta T^2} L + \frac{S}{\beta T}(C_w - C_i) + Ci. \quad (2)$$

Here, S is the sea ice salinity, L is the latent heat of fusion, C_w and C_i are the heat capacities for water and pure ice, respectively, and $\beta = -0.0182°\mathrm{C}^{-1}$. The second term in (1) represents the heat transported by advection of brine upward through the ice during flooding events. Wicking of brine up into the snow is neglected. To account for the phase change that occurs as brine is transported along temperature gradients in the ice, C_b also includes a latent heat term. C_b is most readily obtained from (2) by setting S equal to the brine salinity.

The second term on the right in (1) represents the absorption of shortwave radiation in the medium (Beer's law). Here, κ is the bulk extinction coefficient of light in the snow or ice, I_o is the net radiative flux at the surface, and z is the vertical depth. Strictly speaking, Beer's law is valid only for monochromatic light in an infinite medium. In the upper part of the snow cover, longer wavelengths are strongly absorbed. To accommodate this, we follow the practice of *Maykut and Untersteiner* [1971] and define I_o as the fraction of radiation that penetrates beneath 10 cm. Below this depth κ is fairly constant [*Choudhury*, 1981], and exponential decay becomes a reasonable approximation. I_o is estimated based on the parameterization of *Grenfell* [1979]. This treatment is somewhat oversimplified; however, as this study concentrates primarily on the dark winter months, the effects of shortwave absorption on the heat balance of the ice are minimal.

Equation (1) assumes that the solid matrix and fluid are in thermal equilibrium, which may be true only for quite slow flow rates. As equation (1) is general, it applies to the snow cover as well as the ice below. Since we are concerned only with the fall and winter months, freshwater infiltration and snowmelt are not treated, although this may be an important process in the outer ice pack [*Sturm et al.*, 1998].

Ice growth at the base of the ice is given by

$$k_{si} \frac{dT}{dz} = \rho_{si} L_{si} \frac{dz}{dt} + F_w, \quad (3)$$

where L_{si} is the latent heat of fusion for sea ice and F_w is the oceanic heat flux due to heat transfer from the upper ocean to the ice. F_w is assumed to be 5 W m^{-2}. Temperature and salinity of the ocean are assumed to be -1.85 °C and 35‰, respectively. Material properties for (1) and (3) are taken from *Yen* [1981]. At the surface of the snow (or ice) the temperature is determined by balancing the surface heat fluxes [*Maykut*, 1978]:

$$F_l + F_E + (1 - \alpha)F_r - I_o + F_s + F_e + F_c = 0, \quad (4)$$

where F_l is the incoming long wave radiation, F_E is the emitted long wave radiation, F_r is the incoming shortwave radiation, F_s and F_e are the sensible and latent heat fluxes, respectively, F_c is the conductive heat flux, and α is the albedo. The albedo of snow-free ice is taken from *Weller* [1972]. The albedo of ice with a snow cover is estimated from the measurements of *Allison et al.* [1993]. F_l is estimated by [*Key et al.*, 1996]

$$F_l = \sigma T_a^4 (0.746 + 0.0066e)(1 + 0.26C), \quad (5)$$

where T_a is air temperature, σ is the Stefan-Boltzmann constant, e is the vapor pressure (mbar), which is computed for an assumed relative humidity of 0.9, and C is the relative cloud cover, taken as 0.7. The shortwave radiation is computed after *Zillman* [1972], modified by a cloud factor of $1 - 0.6C^3$ [*Maykut*, 1978]. The turbulent fluxes are calculated from the standard bulk transfer parameterizations [e.g., *Maykut*, 1978], with bulk transfer coefficients taken from *Cox and Weeks* [1988].

2.2. Snow Model

As the snow cover provides both very effective insulation for the ice as well as the necessary load to depress the ice for flooding to occur, the treatment of processes

in the snow cover is critical for proper modeling of both congelation ice growth and the flooding/snow ice formation process. Since ice brine volumes and desalination processes are dependent on the thermal regime of the ice, the permeability, and hence flooding processes, are highly dependent on modeled snow/ice interface temperatures. Heat transfer through the snow cover is highly dependent on diagenesis in the snowpack [*Sturm et al.*, 1998]. The key processes of relevance to the present study are the mechanical deformation and diagenesis of the snow cover, including destructive metamorphism, such as the density increase due to settling and compaction, constructive metamorphism due to grain growth and depth hoar formation, and melt metamorphism in saturated snow and slush at the base of the snowpack. Depth hoar is a ubiquitous feature of the snowpack over sea ice in the Ross Sea region [*Sturm et al.*, 1998], and owing to its very low thermal conductivity, its formation is an important process in controlling the heat transfer through the snowpack. However, predicting production rates of kinetic growth grains is difficult [*Colbeck*, 1983; *Sturm*, 1991], particularly so in this case where the base of the snowpack is often infiltrated by brine [*Sturm et al.*, 1998], which will affect the vapor transfer and crystal growth processes which control depth hoar formation. Because of these difficulties, depth hoar formation is not treated in the model. The possible consequences of this simplification are discussed below.

For densification due to settling, we use the formulation of *Anderson* [1976],

$$\begin{aligned} \frac{1}{\rho_s}\frac{d\rho_s}{dt} &= 2.8\times 10^6 e^{0.04T} e^{-46(\rho_s-150)} \\ &\qquad \rho_s > 150\ kg\ m^{-3}, \\ \frac{1}{\rho_s}\frac{d\rho_s}{dt} &= 2.8\times 10^6 e^{0.04T} \\ &\qquad \rho_s < 150\ kg\ m^{-3}, \end{aligned} \tag{6}$$

where ρ_s is the snow density (kg m^{-3}) and T is the temperature (°C). For densification due to compaction, we have [*Anderson*, 1976]

$$\begin{aligned} \frac{1}{\rho_s}\frac{d\rho_s}{dt} &= \frac{W_s}{\eta} e^{0.021\rho_s}, \\ \eta &= 1\times 10^7 e^{(0.081T)}, \end{aligned} \tag{7}$$

where W_s is the weight of the overburden and η (N s^{-1}) is the viscosity of snow. The initial density of new snow, 254 kg m^{-3}, is based on measurements of recent snow by *Sturm et al.* [1998]. This value was chosen as low-density, new snow was rarely observed in the study region, and the prevalence of high winds would tend to increase the rate of densification of new snow.

The most critical parameter in the snow cover model is the thermal conductivity. Commonly, it is expressed as an effective thermal conductivity to account for both heat transport due to conduction and vapor diffusion. This has been the subject of extensive study, both theoretically and experimentally [*Arons and Colbeck*, 1995; *Sturm et al.*, 1997]. Here we use the equations given by *Sturm et al.* [1997],

$$\begin{aligned} k_s &= 0.138 - 1.01\times 10^{-3}\rho_s + 3.233\times 10^{-6}\rho_s^2 \\ &\qquad 156 \le \rho_s \le 600 \\ k_s &= 0.023 + 0.234\times 10^{-3}\rho_s \\ &\qquad \rho_s < 156, \end{aligned} \tag{8}$$

where ρ_s is the snow density in kg m^{-3} and k_s has units of W m^{-1} K^{-1} . The uncertainty in (8) is ±0.1 W m^{-1} K^{-1}. It should be noted that (8) gives effective thermal conductivities that are generally lower than those given by most other studies. For instance, for typical observed snow densities, (8) gives values about half that of those given by *Abel's* [1893]. This difference may in part be due to the generally lower sample temperatures for the measurements of *Sturm et al.* [1997].

For slush, the thermal conductivity is calculated using a Maxwellian model [*Schwerdtfeger*, 1963],

$$k_{\text{wet}} = \frac{2k_i + k_b - 2v_b(k_i - k_b)}{2k_i + k_b + v_b(k_i - k_b)} k_i, \tag{9}$$

where k_i and k_b are the thermal conductivities of ice and brine, respectively, and v_b is the relative brine volume. Such a model is strictly valid only for a continuous ice matrix with small spherical brine inclusions. This is not true for slush, and so (9) may not be accurate. However, for typical slush brine volumes and ice and brine thermal conductivities, (9) gives values of k_{wet} quite close to that of a parallel plate model, so the error in k_{wet} is likely considerably less than the uncertainty in k_s.

Erosion of snow due to wind drifting is not included in the model. While local redistribution is not germane to the mass balance in a 1-D model, loss to neighboring leads is. *Eicken et al.* [1994] estimated that these losses may be more than 10 cm over the course of a year in the Weddell Sea. However, they noted that hardening of the snow surface due to metamorphism may prevent the suspension of particles even in strong winds. *Sturm et al.* [1998] described a similar effect due to icing of the surface snow. In light of the uncertainty in precipitation estimates, we neglect the effects of snow redistribution.

2.3. Salinity Model

The salinity of sea ice is normally governed by three main processes: the initial entrapment of brine during ice formation, the expulsion of brine due to the expansion of the ice as it cools, and gravity drainage [*Weeks and Ackley*, 1986]. In this paper we also investigate a fourth mechanism: upward flushing due to brine percolation through the ice during flooding events.

Initial salt entrapment is given by

$$S_{si} = k_{\text{eff}} S_w, \tag{10}$$

where k_{eff} is an ice growth velocity dependent segregation coefficient, taken from *Cox and Weeks* [1988], S_{si} is the initial salinity (‰) of the new ice, and S_w is the salinity of seawater. As the model formulation is based on the control volume approach [*Patankar*, 1980], the treatment of brine expulsion due to brine freezing in the interior of the ice is quite simple. If the total relative volume of components (ice and brine) within a control volume exceeds unity, the excess volume of brine is moved into the layer below, where volumes are recomputed and the process is then repeated for all ice layers. This treatment is essentially equivalent to the finite difference formulation presented by *Cox and Weeks* [1975]. Note that this does not allow for upward expulsion of brine into the snow cover. This can lead to a wet, saline snow layer at the snow/ice interface which may wick up several centimeters into the snowpack [*Sturm et al.*, 1998].

The most important factor in the evolution of the salinity profile of the ice is gravity drainage. Brine entrapped in sea ice forms a network of interconnected fluid pathways which tend to form elongated tubes that provide connectivity between the entrapped brine and the seawater beneath [*Bennington*, 1967; *Lake and Lewis*, 1970; *Niedrauer and Martin*, 1979; *Cole and Shapiro*, 1998]. Owing to the vertical density gradient of the brine, brine may become convectively unstable within the ice [e.g., *Wooding*, 1959; *Lake and Lewis*, 1970; *Niedrauer and Martin*, 1979]. This causes convective overturn of the brine within the pore space and an exchange of the cold dense brine with underlying seawater. Interception of the brine drainage network by isolated brine inclusions may enhance the rate of desalination [*Bennington*, 1967]. While no mechanistic model is currently available to account for this process, *Cox and Weeks* [1975] provided an empirical relationship based on observations of brine drainage in growing NaCl congelation ice. For brine volumes > 0.05, they give the rate of change of ice salinity (‰) as

$$\frac{dS}{dt} = (1.68 \times 10^{-7} - 3.37 \times 10^{-6} v_b)\frac{dT}{dz}, \qquad (11)$$

where dT/dz is the vertical temperature gradient (°C m^{-1}). For brine volumes < 0.05, the ice becomes impermeable and no brine is drained from above the impermeable layer.

Unfortunately, (11) is not expressed in a conservative form; that is, although it permits calculation of the amount of salt lost from an individual ice layer, it tells us nothing about the brine fluxes between layers which govern the decrease in salinity. Since these fluxes are likely dependent on ice microstructural variations and brine salinity gradients, proper treatment of brine drainage under a variety of natural conditions requires knowledge of how these factors control brine transport. For conditions similar to the experiments from which (11) was determined, namely, growing congelation ice with a constant thermal forcing [*Cox and Weeks*, 1975], the brine exchange should be implicitly accounted for by (11). For natural sea ice, we might expect that large differences in microstructure and porosity and highly nonlinear temperature gradients might affect the nature of this brine exchange so that, for example, brine draining from one layer may increase the salinity of a lower layer, and (11) will no longer adequately describe the salinity evolution of the ice.

Nevertheless, (11) has proven adequate to describe brine drainage in Antarctic sea ice, regardless of ice type [*Eicken*, 1992]. Furthermore, observations of bulk salinities show little difference based on ice structure (M. O. Jeffries, unpublished data, 1995). Presumably, this is because drainage features such as brine tubes form in both granular and columnar ice. Snow ice is similar in texture to frazil ice, and it is likely that, given time, similar drainage features could form in snow ice layers. Because of the current lack of any alternative, equation (11) is used to describe desalination by brine drainage in snow ice as well as columnar ice.

The treatment of brine drainage in the slushy layer is another matter. Although the slush forms a porous matrix similar in structure to frazil ice, the high brine volumes make it considerably more porous than most granular ice layers. Thus in contrast to congelation and granular sea ice, all the pores are well connected, and brine drainage may be enhanced. However, unlike in congelation and granular sea ice, there is likely a great contrast between the permeability of the slushy layer and that of the ice below; consequently, transport of brine draining from the slush into the underlying ice may be impeded. Furthermore, convective overturn of brine as the slush layer refreezes may be sufficiently vigorous to affect the heat budget of the slush layer and the underlying ice. Therefore the proper treatment of brine drainage from the flooded layer may require coupling of the equations for brine drainage and heat flow [e.g., *McGuinness et al.*, 1998]. However, since proper treatment of this problem is prohibitive in a simple 1-D model, equation (11) is applied to the slushy layers as well. The weaknesses and consequences of this treatment of brine drainage are discussed in detail below.

2.4. Flooding and Brine Flow

When the snow load on the ice is sufficient to depress the ice surface below sea level, there is the potential for seawater or brine to infiltrate to the ice surface and flood the base of the snowpack. This condition is met when the freeboard becomes negative. The freeboard is calculated from the equation for isostatic balance,

$$fb = \frac{(\rho_w - \rho_{si})}{\rho_w} Z_{si} - \frac{\rho_s}{\rho_w} Z_s, \qquad (12)$$

where fb is the freeboard, ρ_w and ρ_{si} are the densities of seawater and sea ice, respectively, and Z_{si} and Z_s are the ice and snow thicknesses, respectively.

Although a negative freeboard is a necessary requirement for flooding of the ice surface, it is not a sufficient one. There must also exist pathways for brine and seawater to infiltrate from the lower ice layers and the sea below into the snowpack. In the percolation model, we require the ice to be permeable throughout its entire thickness.

The pore space geometry in sea ice is complex and spatially and temporally inhomogeneous. In congelation ice, brine is trapped between ice lamellae as the ice grows, and tends to form oblately tubular inclusions along plate and crystal boundaries [e.g., *Bennington*, 1967; *Perovich and Gow*, 1996; *Cole and Shapiro*, 1998]. These may be a few millimeters long with poor connectivity in cold ice [*Cole and Shapiro*, 1998] or a centimeter or more long and well connected in warm ice [*Weissenberger et al.*, 1992]. In very warm ice the brine space may be well connected along crystallographic boundaries [*Perovich and Gow*, 1996, Figure 10]. In frazil ice the entrapped brine forms a convoluted network of pathways along the grain boundaries [*Weissenberger et al.*, 1992, Figure 3]. Brine drainage tubes provide permeability either on a small scale, via the interconnected tubules along grain and plate boundaries, or by second-generation tubules which have cut across these boundaries [*Bennington*, 1967], or via large-diameter roughly vertical tubes with radial feeder structures [*Lake and Lewis*, 1970; *Cole and Shapiro*, 1998]. The pore structure of sea ice is illustrated in Figure 2. Large drainage tubes may provide a high, localized permeability; however, the bulk material also has a permeability due to the sea ice substructure (blowup diagram). *Golden et al.* [1998] have suggested that the permeability of sea ice is due primarily to this substructure near the percolation threshold. Permeability may also be provided by brine "corrosion bands" in small cracks and fissures caused by thermal cracking [*Bennington*, 1963], or by large-scale cracks caused by ice deformation. All these features may form parts of an interconnected network of pore space that may or may not render the ice permeable, either in the bulk pore space, through individual drainage tubes, or in spatially restricted areas of cracked or high-porosity ice. The pore network, and hence the permeability may change dramatically depending on the thermal history of the ice even without significant transport of brine.

Figure 2 shows a representation of the mechanism for brine and seawater percolation. At equilibrium the brine within the ice is at its in situ freezing point. If a temperature gradient exists through the ice, any transport of brine along the gradient will result in heat transfer between the brine and ice and there will be phase change. Warmer, fresher brine moving up through a brine channel in the ice, despite carrying with it sensible heat, will tend to freeze against the walls of the channel as it loses heat to the colder ice, as observed by *Niedrauer and Martin* [1979]. They observed melting on one side of the channel as cold brine descended, while warm brine moved up the other side of the channel, plating it with ice. Under the influence of a potential head (due to the depression of the ice surface below sea level), seawater will begin to move up through the ice, provided it is permeable, displacing the colder, denser brine ahead of it, and thus modifying the salinity structure of the ice. The warm brine will lose heat to the colder, surrounding ice, freezing against the walls of the conduits and concentrating the brine. This freezing will restrict the fluid pathways, perhaps even closing them off, thus reducing the permeability of the ice. The release of latent heat will warm the ice adjacent to the channel, and heat will flow laterally along the temperature gradients (Figure 2). This heat transfer will warm the isolated brine pockets which, in turn, will grow in size by self-dilution, and they may coalesce and form additional hydraulic pathways. In this way the porosity and permeability of the ice are closely coupled with the flow itself. It should be stressed that while the influx of warm brine will tend to warm the ice and increase the brine volume, the infiltrating seawater is at its in situ freezing point. The only way it can transfer heat to warm the ice is by partially freezing. Then the overall effect will be to reduce the brine volume.

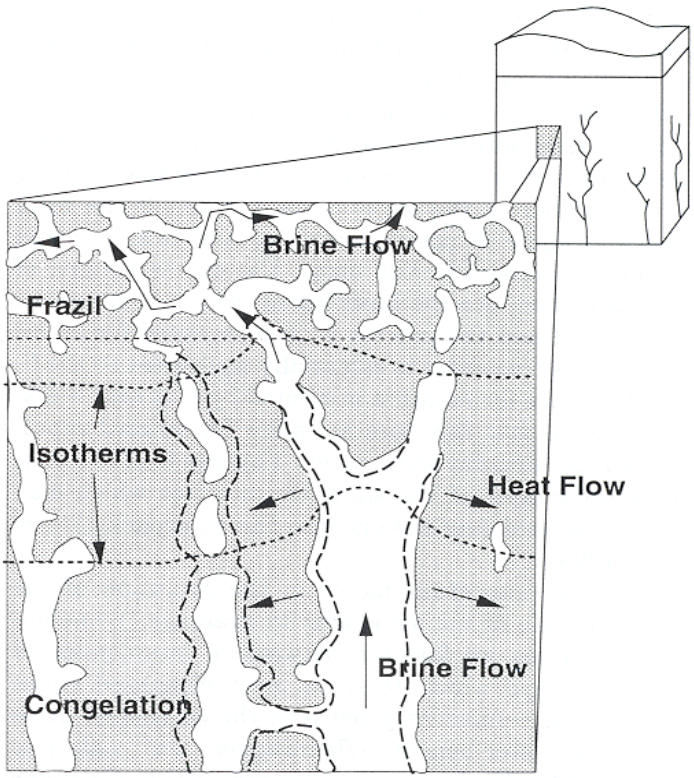

Figure 2. Schematic representation of the porous structure of sea ice and model of brine transport. During upward flow of brine, the isotherms (dotted lines) are displaced vertically, and there is heat flow from the brine channel to the ice and isolated pores. This causes freezing and narrowing of the channel and a corresponding enlargement of the unconnected pores, indicated by the dashed lines.

Obviously, solving the equations of fluid flow for such a complicated and essentially unknowable geometry is impossible. However, the average macroscopic flow may be described using Darcy's law [*Bear*, 1972]

$$u_d = \frac{K}{\mu}(\rho_b g - \nabla P), \tag{13}$$

where u_d is the area-averaged fluid velocity, which is related to the pore fluid velocity by

$$u_d = \phi u, \tag{14}$$

K is the intrinsic permeability, μ is the fluid viscosity, and ∇P is the pressure gradient due to the depression of the ice surface below sea level. Then, brine and salt transport may be expressed as

$$\begin{aligned} \frac{dM_b}{dt} &= \frac{d}{dz}(u_d \rho_b), \\ \frac{dM_s}{dt} &= \frac{d}{dz}(u_d \rho_b S_b), \end{aligned} \tag{15}$$

where M_b and M_s are the masses per unit volume of brine and salt, respectively, ρ_b is the brine density, and S_b is the brine salinity. In this way we need not know any details of the flow geometry provided we have a suitable method for estimating the permeability, assuming that the flow is homogeneous when averaged over a sufficiently large area.

Estimates for the permeability of sea ice are scarce. *Ono and Kasai* [1985] measured permeability in natural sea ice and observed a curious anisotropy in measured upward and downward permeabilities. This may be due to effects of the flow on the porosity; however, the results are the reverse of that expected. Unfortunately, they did not report brine volumes, and so any correlation between permeability and porosity is impossible to determine. *Saito and Ono* [1978] also did not report brine volumes; however, they may be crudely estimated based on the conditions under which the ice was grown. Figure 3 shows a plot of permeability measurements from several authors plotted against estimated brine volumes. The solid line shows a least squares third-order polynomial fit to the log transform of the data which were used to determine the permeability in the model. Note that only the data shown for the studies by *Saeki et al.* [1986] and *Kuroiwa* [1968] were used for the fit, as only these studies reported porosities. The brine volumes for the other two studies were estimated from the reported growth conditions and are shown only for reference. The most common parameterization relating porosity and permeability is the Kozeny-Carman equation [*Bear*, 1972],

$$K = \frac{d^2}{180}\frac{v_b^3}{(1 - v_b^2)}, \tag{16}$$

where d is a representative grain size. This may not be valid for columnar ice, in which the permeability may be controlled by vertical drainage tubes, but may be reasonable for granular ice, which, since it will generally be present in the upper portions of an ice floe, is the controlling factor for the overall ice permeability. The Kozeny-Carman relation for a grain size of 1 mm is shown in Figure 3 as a dashed line for comparison. There are pitfalls with this approach in that permeability is likely to be dependent not only on the porosity, but also on the thermal and brine flow history of the ice.

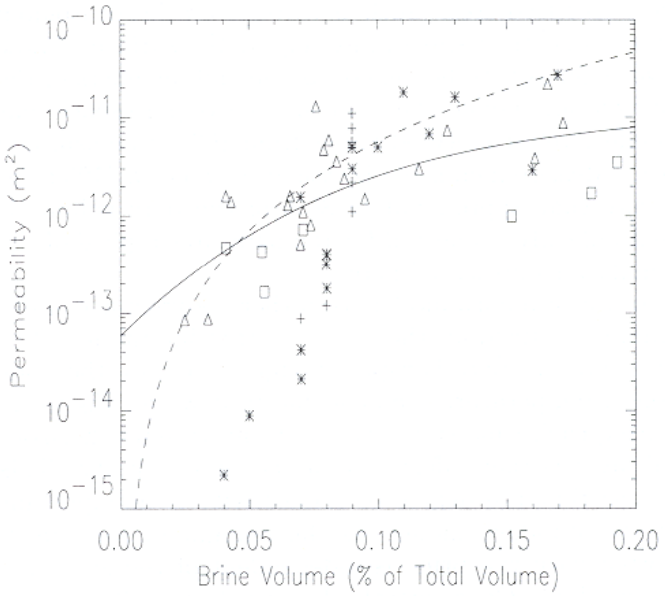

Figure 3. Dependence of sea ice permeability on estimated relative brine volume. Data are from the following sources: asterisks, *Ono and Kasai* [1985]; triangles, *Saeki et al.* [1986]; pluses, *Saito and Ono* [1978]; and squares, *Kuroiwa* [1968]. The data from Kuroiwa are for artificially compressed snow. The solid line represents a best fit to the data. The dashed line is a fit of the Kozeny-Carman equation for a grain size of 1 mm [*Bear*, 1972].

In light of the uncertainty in the brine percolation process, we explore two possibilities: (1), a standard model, where brine advection in the ice is governed by (13) and (15), and (2), a simple model, where flooding takes place by direct infiltration of seawater into the snowpack, and (15) is not used (there is no internal displacement of brine within the ice). To retain consistency, (13) is still used to determine the infiltration rate. In the standard model, the bulk of the pore space is effectively connected, so, as the brine is advected upward, the higher-salinity brine ahead of it is flushed from the ice. This implies that the ice is reasonably horizontally homogeneous, so that the flow is essentially uniformly distributed throughout the ice sheet when averaged over a sufficiently large area. In the simple model, brine within the sea ice is isolated from the network of pathways through which flooding takes place, so there is no advection of brine or heat through the ice sheet. This would be the case if the flow was confined to only

very localized areas, such as through cracks, or isolated tubes, and then spread laterally at the surface. These two regimes may be viewed as the end-members of the percolation model where the amount of pore space that is effectively connected varies from 100% to essentially 0%. Measurements by *Weissenberger et al.* [1992] indicate that approximately 80% of the pore volume is hydraulically connected for temperatures typical of the simulations presented here.

In the standard model, local thermodynamic equilibrium is assumed for the sea ice so that lateral heat flow from pore to pore is rapid enough to remove the horizontal temperature gradient due to flow (see Figure 2) during each time step. All the brine within a horizontal layer is then effectively of the same salinity. This means that the degree of connectivity is unimportant in the standard model, as the amount of salt transported with the brine is independent of the geometry of the flow. Consequently, brine volumes after a flow event will be the same regardless of the effective porosity. If the flow is restricted spatially, such as in isolated drainage tubes, the fluid pore velocity is proportionately higher, and horizontal temperature gradients will exist. In this case, brine salinities in the bulk of the pore space remain higher than those in the pore space in which most of the flow is taking place, and less salt is flushed from the ice. The simple model is the extreme case of this regime. This implies that the percolation threshold (and the permeability) will likely not be solely a function of brine volume, but will be time dependent, depending on the evolving pore geometry. In this study, however, the critical porosity for percolation is assumed to be constant at 5%.

As the flooded layer freezes, compositional (salinity) and temperature gradients may exist within the slush. Freezing may then occur over the entire thickness of the slush as it solidifies. This is akin to the so-called "mushy layer" problem that has received much attention in metallurgy [e.g., *Worster*, 1986]. As the brine freezes, it rejects salt into the melt, thus concentrating the brine and allowing the slush to cool further, so that the temperature gradient propagates down through the slush and underlying ice, solidifying the slush throughout its thickness. Observations indicate, however, that convection of brine as the slush freezes is quite vigorous [*Lytle and Ackley*, 1996; *Hudier et al.*, 1995]. In this paper we assume that the salt rejected during freezing drains quickly, so that the brine salinity at the freezing interface remains constant, as is the case at the ice/ocean interface. Therefore the temperature of the slush and ice is held constant by the eutectic condition until the entire slush layer freezes. The freezing interface is defined across a layer of finite thickness at the top of the slush layer. When this uppermost layer of slush reaches a solid fraction of 0.6, it is assumed to be frozen, and the freezing interface is moved down to the next layer. Note that this does not imply that the slush and underlying ice temperatures and brine salinities are those of the underlying seawater, but rather that they are determined by the upward transport of heat and salt during the flooding event, as indicated by (13) and (15). This can lead to very high salinities in the flooded layer, as has been observed in the field [*Sturm et al.*, 1998].

2.5. Numerical Solution

The system of equations (1), (3), and (13) and (15) are solved using a finite volume method [e.g., *Patankar*, 1980], so that the quantities of interest (masses of salt, brine, and ice) are conservative. Although this essentially reduces to a finite difference method, mass of brine and mass of salt are the primary variables, rather than salinity. Equation (1) is solved using a semi-implicit scheme similar to that of *Goodrich* [1978] and *Wade* [1993]. Equation (15) is solved using a first-order upwind scheme. Layer thickness is nominally set to 2 cm. The bottom ice layer is of variable thickness so that the growth interface is tracked continuously. The snow layer thicknesses are also variable to accommodate densification. For each time step, first the brine velocity is determined from (13). The energy equation, (1), is solved, and the mass transfers of salt and brine are calculated from (15). Then, change in salt content due to brine drainage and expulsion is computed. There is assumed to be no brine drainage during a flooding event. The masses of ice and brine are then updated for each layer based on the temperature and salinity following *Cox and Weeks* [1975]. In this way the equations for heat and mass transfer are decoupled and can be calculated independently for each time step. A time step of 0.5 hours is used when there is no upward brine flow and is reduced accordingly when there is brine flow. Verification of the solution technique by comparison of a simplified model with the analytic solution to the Stefan problem [*Hill*, 1987] showed agreement to within less than one layer thickness.

Air temperature forcing fields were taken from automatic weather station data for Possession Island (71.9°W 171.1°E), as this was deemed the most representative and reliable data set for the region of interest that was continuous over the study period (April - November 1995) and most likely represents typical values for the region of the Ross Sea for which field measurements were taken [see *Jeffries et al.*, 1998a]. Although this station is quite close to the continent, and may not be truly representative of the ocean regions, temperatures were in reasonable agreement with shipboard observations. Snow accumulation data was estimated using National Centers for Environmental Prediction (NCEP) reanalysis precipitation rates, for the same time period and approximate location (71.4°S, 180°E). The total accumulation was scaled to give a yearly total of 400 kg m^{-2}, water equivalent, based on estimated precipitation rates for the Ross Sea [*Giovinetto et al.*, 1992]. The wind speed was set to 10 m s^{-1}. The effects of variation in the climatic forcing are discussed below. Simulations

were run for climatic conditions for 1995, so that the results might be compared to field data from one autumn and one winter cruise in the Ross Sea in 1995 aboard the R/V *Nathaniel B. Palmer*.

3. Results

3.1. Flooding and Snow Ice Formation

Figure 4 illustrates model results for both the normal model (Figure 4a) and the simple model (Figure 4b) for ice growth initiating on May 1 (Julian day 121). Ice growth is initially very rapid, with thicknesses approaching 40 cm within a few days. Once a snow cover has developed, however, little congelation ice is added throughout the growth season. This is particularly true for the standard model, which produces only 6 cm of congelation ice during the last 5 months of growth, for a total of 52 cm. During the period of flooding and snow ice formation, approximately 4 cm of ice is melted from the bottom before the temperature gradient is reestablished. In the simple model, there is very little bottom melting; however, repeated flooding events keep the ice warm, preventing any substantial congelation ice growth.

Brine volumes are consistently above the critical value of 5% for the early stages of growth, except for a brief interval before significant snow accumulation. This is primarily due to the insulation provided by the snow cover, which maintains the ice at quite high temperatures. The average snow/ice interface temperature for the simulation in Figure 4a was -4.3°C. This is much higher than the average observed value of -9.8°C (M. O. Jeffries, unpublished data, 1995), in part due to the relatively thin ice (mean, 53 cm, of which 5 cm was snow ice) and deep snow (mean, 32 cm). The simple model produced more typical values of snow and ice thickness, with a mean ice thickness of 66 cm, including 17 cm of snow ice and mean snow depth of 22 cm. However, the average interface temperature was still quite warm (-4.4°C). For comparison, the mean ice thickness from the two winter cruises was 64 cm, with a mean snow ice thickness of 17 cm. Snow depths averaged 16 cm.

The process of flooding and snow ice formation produces quite different results for the two regimes. First, in the standard model, after the initial flooding the slush layer persists for several days before freezing. The rate of freeze-up is very slow, since unless a cold front moves down through the ice, the brine salinity must be decreased by brine drainage for freezing to occur. In the simple model, freeze-up of slush is quite rapid, owing to the relatively low salinity of the incoming seawater. Some of this seawater is frozen initially upon contact with the cold snow, and as the temperature gradient is reestablished through the ice and snow after flooding, the low-salinity slush freezes quite readily. As a result, a slush layer often never really exists.

In terms of mass balance, the difference between the two flooding regimes is quite important. First, in the standard model, upward flow of brine through the porous brine network in the ice flushes more saline brine up onto the ice surface, replacing it with warmer, less saline brine. As the flooded layer freezes and the ice below cools again, the brine volume is correspondingly decreased, as shown by the impermeable layer in Figure 4a (see also Figure 5d). On day 195 the brine volumes

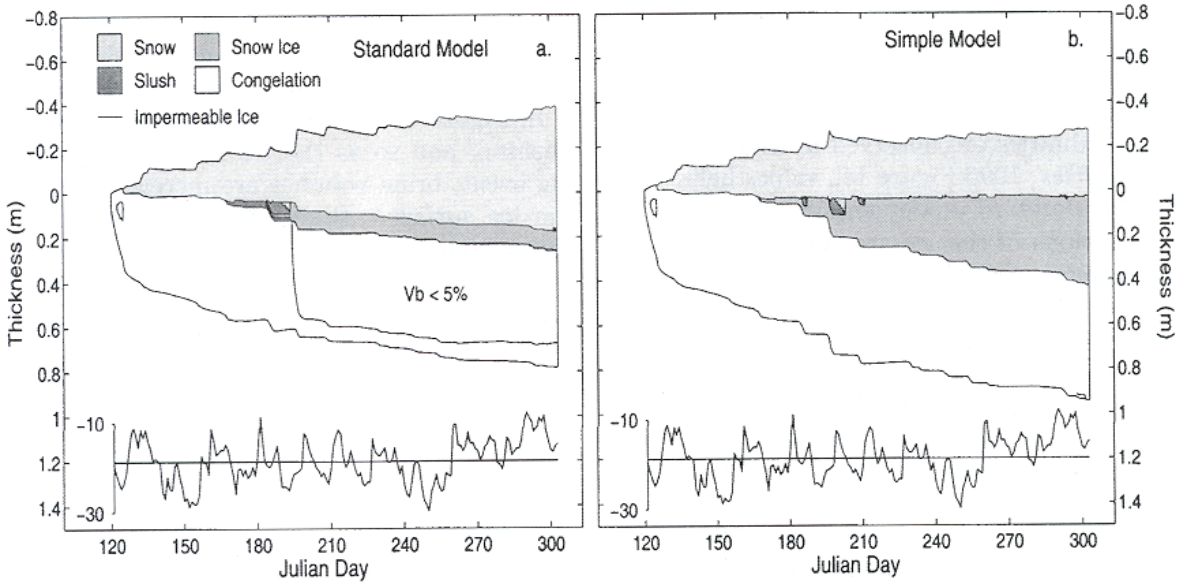

Figure 4. Simulated time series of sea ice growth in the Ross Sea. (a) Standard model, including internal brine flow in the ice. (b) Simple model, without internal brine flow. The region of impermeable ice is indicated by the solid contours within the congelation ice layer. Depth is relative to sea level. Also shown is a trace of the air temperature (°C) record from AWS98495 (Possession Island).

in the congelation ice drop below the assumed critical value for permeability of 5% and remain below this value throughout the bulk of the congelation ice for the remainder of the simulation. Therefore despite a negative freeboard, no further flooding or snow ice formation occurs. In contrast, in the simple model, where there is no upward flushing of brine, the brine volumes in the lower ice layers remain above the critical value for most of the simulation period, allowing repeated flooding and greater snow ice formation.

3.2. Salinity and Brine Volume

The effects on salinity and brine volume are more readily seen in Figure 5, which illustrates the vertical salinity profile for the standard and simple models. For comparison, three salinity profiles taken from ice cores sampled during the two cruises aboard the R/V *Nathaniel B. Palmer* in 1995 [*Jeffries et al.*, 1998a] are shown in Figure 5c. The profiles are taken from cores sampled on Julian days 157, 218, and 227. They were chosen because they consisted of a single layer of congelation ice topped with one or more layers of granular ice that can reliably be assumed to be snow ice due to their highly negative $\delta^{18}O$ values [*Jeffries and Adolphs*, 1997]. We can therefore expect that these cores experienced growth processes comparable to those in the simulations.

In Figures 5a and 5b we see that the profiles are generally S-shaped or slightly C-shaped [*Eicken*, 1992]. Brine drainage is quite efficient, and salinities decrease to below 5‰ in the lower portions of the ice before flooding occurs (day 165). This is due primarily to the insulating effect of the snow cover, which warms the ice and maintains high brine volumes even for low-salinity ice. This allows for efficient brine drainage, according to (10), despite small temperature gradients. As brine drainage will continue as long as brine volumes are greater than the threshold value of 5%, there will be brine drainage even for quite low salinities in warm ice. While low salinities are observed in ice cores [e.g., *Maksym and Jeffries*, 1996,Figure 1c], values below 3‰ are rare. In the standard model simulations, salinities in the lower portions of the ice are consistently below 3‰, largely because of the anomalously warm ice. In the standard model, there is a substantial drop in salinity during the main flooding event, as illustrated by the difference between profiles at day 165, before any flooding, and day 175, after the first flooding event. There is a drop in salinity throughout the entire ice thickness, but it is most pronounced at the top of the congelation ice layer, where the effects of upward brine flushing are greatest. After freeze-up of the flooded layer (day 195), a pronounced "knee" is evident in the salinity profiles between the congelation and snow ice layers, with very high salinities in the snow ice layer (15-20‰), and quite low (~3‰), nearly uniform salinities in the congelation layers. There is little change in the salinity after day 195, when freeze-up is complete, and the ice remains impermeable. The simple model shows similar salinities in the snow ice layers (approximately 15-17‰). However, the congelation ice layers show little change in salinity after flooding due to the lack of upward flushing. Brine drainage from these layers is reduced as the brine volumes approach the critical cutoff value of 5% (Figure 5e). Salinities at the base of the ice decrease primarily because of reduced ice growth rates, so initial brine entrapment is reduced [*Cox and Weeks*, 1988]. The salinity profiles from the simple model provide a closer match to the field data in Figure 5c in terms of overall shape and salinity in the lower portions of the ice.

Brine volumes for the standard model, simple model, and field data are presented in Figures 5d, 5e, and 5f, respectively. Figure 5d shows brine volumes just prior to flooding (day 165), after flooding (day 175), and after freeze-up and cooling (day 195). After the flooding event there is a slight decrease in brine volume in the lower congelation ice layers, despite the warming of the ice. This is caused by heat conduction maintaining a slight temperature gradient through the ice even as the brine moves upward, cooling this brine as it moves, causing some of it to freeze. After the ice is allowed to cool again and the temperature gradient is fully restored, brine volumes are significantly reduced (day 195). Note that brine volumes drop to well below the critical value for permeable ice (5%) despite the ice being very warm (> -4°C). This means that the ice is unlikely to become permeable again even with warmer air temperatures, unless the salinity is increased in some way. The enhanced reduction in brine volume at the top of the congelation ice layer is caused by flushing of brine from this ice combined with significant warming of the ice during flooding. Once the ice cools again, it is the ice at the top which cools the most, producing very low brine volumes. This produces the curious result that some of the lowest brine volumes in the ice often occur immediately adjacent to some of the highest.

In Figure 5e, for the simple model, there is no brine flushing, and so as the ice is warmed during a flooding event, brine volumes are increased, especially near the ice surface. High brine volumes are maintained throughout the growth season in part because repeated flooding events continually warm the ice surface. Both models have very high brine volumes in the snow ice layers (approximately 15-25% for the simple model, 20-35% for the standard model). Neither model matches the field data particularly well (Figure 5f). This is due to the much colder temperatures of the ice cores (compare Figures 5g and 5h with Figure 5i). The average ice surface temperature for the three selected cores chosen was -10.4°C, whereas ice surface temperatures averaged only -4.3°C and -4.4°C for the standard and simple models, respectively.

3.3. Effect of Initial Ice Formation Date

The effects of varying the initial ice formation dates, and thus duration of ice growth, are illustrated in Fig-

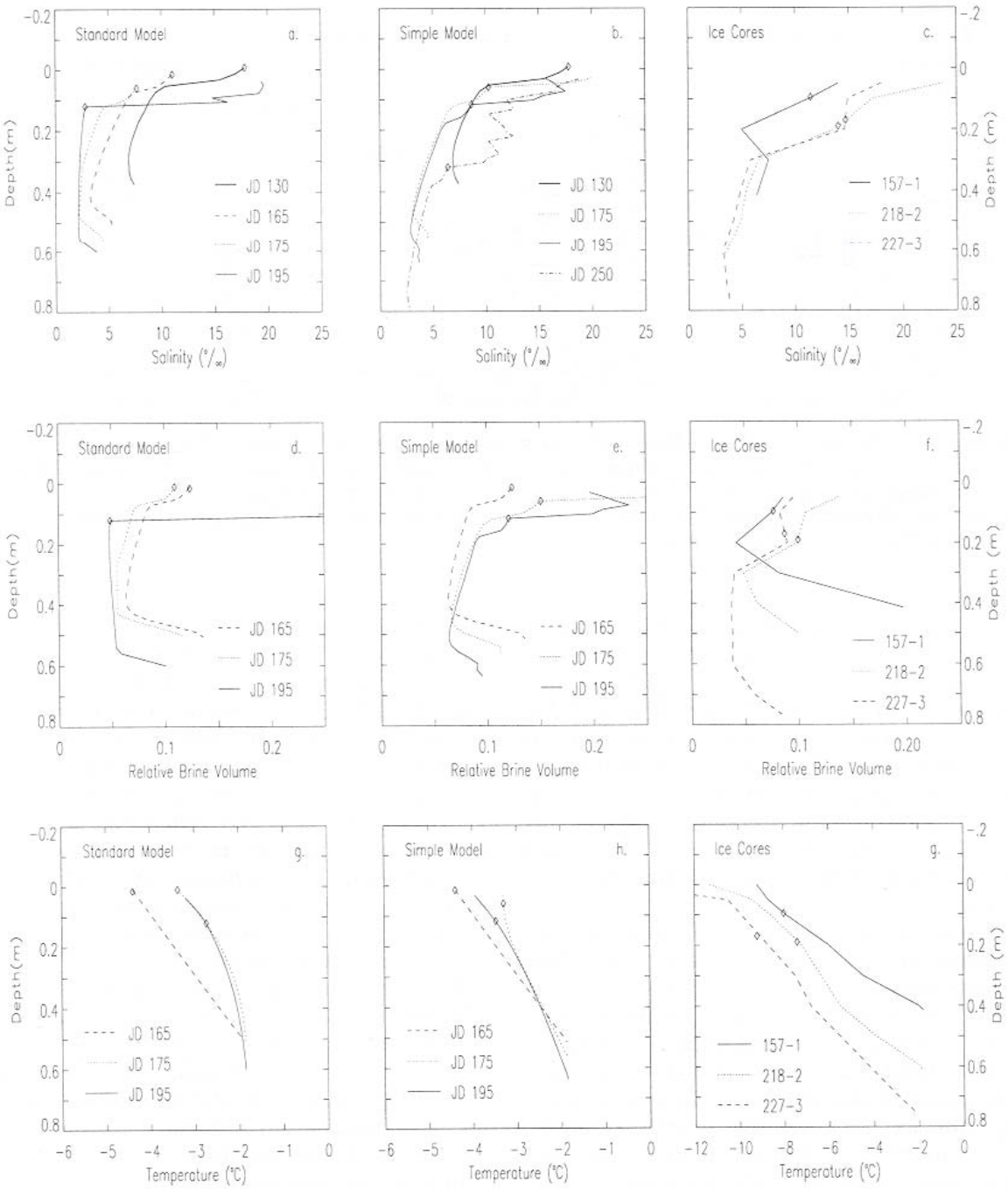

Figure 5. Vertical salinity, brine volume, and temperature profiles for the standard model (Figures 5a, 5d, and 5g respectively), simple model (Figures 5b, 5e, and 5h), and selected ice cores (Figures 5c, 5f, and 5i). Simulation results are shown for several different dates, as indicated by Julian day (JD), to show ice properties before and after major flooding events (refer to Figure 4). Core data (Figures 5c, 5f, and 5i) labels indicate date of sampling and identification number of core taken on that date. The depth scale is relative to the ice surface. The congelation/snow ice interface is indicated on each profile by the open diamond.

ure 6. The total amount of each type of ice present at the end of the simulation (Julian day 304) is presented. The mean values in Figure 6a and 6b are the thicknesses of each ice type averaged over the entire growth period and over each start date. Note that this differs from the mean values at the end of the simulation. Also shown are the mean thicknesses of ice from all ice cores sampled in the Ross Sea during the two cruises aboard the R/V *Nathaniel B. Palmer* in 1995. Note that for these data, frazil and congelation ice are combined and represented as congelation only. Figure 6a shows results for the standard model, and Figure 6b shows those for the simple model. For both flow regimes the amount of congelation ice is almost completely independent of

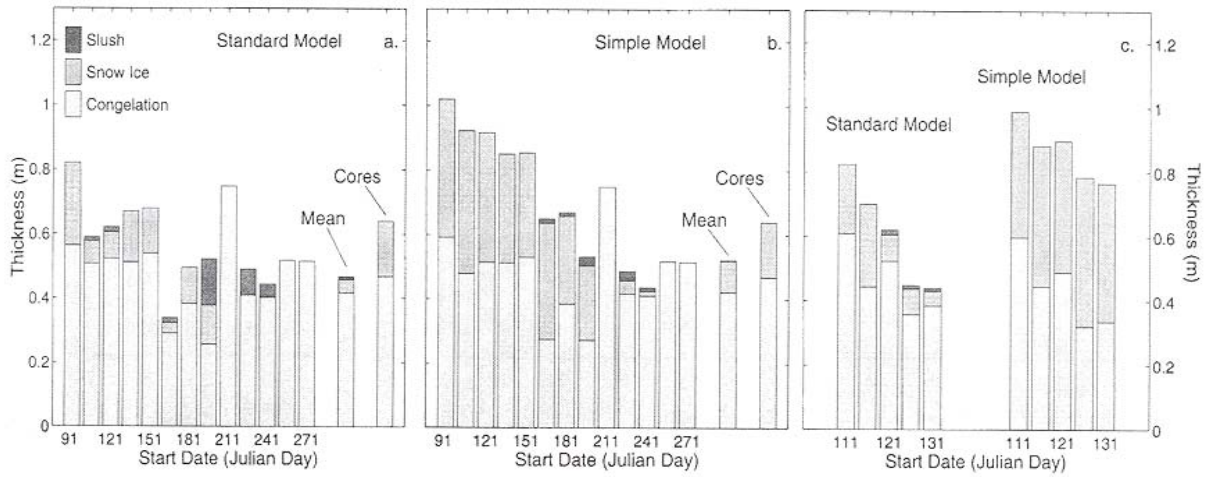

Figure 6. Thicknesses of congelation ice, snow ice, and slush at the end of the simulation period for various start dates for (a) standard model, (b) simple model, and (c) both models with a narrow range of start dates. Climatic forcing is the same as for Figure 4. The bars labeled "mean" are the mean simulation thicknesses for all simulations. The bars labeled "cores" are the mean thicknesses from field data.

initial freezing start date, despite a sevenfold variation in the duration of ice growth. This reflects the fact that initial congelation growth is quite rapid, but once a significant snow cover forms, congelation growth becomes a very slow process, or there may actually be melting from the ice bottom, as is the case in many of the standard model simulations. Once the ice has thickened to approximately 40 cm, the bulk of any further ice thickening is by snow ice development. This value is obviously a function of the climatic forcing, however, and is discussed below.

For the simple model, there is an obvious decrease in total ice thickness as a function of start date. Brine volumes are consistently above the critical value of 5%, and freezing of the slush is quite rapid; hence snow ice develops readily as more snow accumulates. As the ice is generally permeable, snow ice formation is primarily a function of total snow accumulation. In general, there will be more snow ice the longer the growth period. In contrast, the amount of snow ice formed by the standard model does not necessarily reflect the length of the growth period. It reflects the dependence of snow ice development on the timing of the flooding event. An early flooding event may flush enough brine from the lower ice layers to render the ice impermeable after the temperature gradient is reestablished, thus inhibiting further flooding. The low quantities of snow ice for later start dates merely reflect low total snow accumulation.

Mean quantities of congelation ice produced in the simulations compare fairly well with observed values. The mean quantities of snow ice produced by the simulations are, however, less than those observed, considerably so for the standard model. Caution must be exercised in comparisons with field data due to the uncertainty in actual growth conditions and since the sampled ice was subjected to substantial dynamic forcing, which is not accounted for in the model. Although the majority of the ice cores were taken from level ice areas, most consisted of multiple layers [*Jeffries and Adolphs*, 1997], which we attribute primarily to rafting events. While this will make the ice thicker than would otherwise occur for purely thermodynamic growth, we note that most of the rafting events occurred when the ice is relatively thin and such events are rare when the ice is thicker than 40 cm [*Worby et al.*, 1996; *Jeffries and Adolphs*, 1997; *Jeffries et al.*, 1997]. As the simulated ice reaches this thickness very rapidly, the effects of rafting may be relatively minor in determining the long-term thickness of the ice.

The results of simulations run with a narrow range of start dates for both models are shown in Figure 6c. Results are shown for five simulations with ice growth initiated at 5 day intervals. Despite such a narrow range the standard model showed as much variation for both congelation and snow ice layer thickness as for the much broader distribution in Figure 6a. The simple model displayed similar variations in the congelation layer thicknesses, but the final snow ice layer thickness remains nearly constant, regardless of start date. This demonstrates that congelation ice thickness is strongly dependent on conditions during the early stages of growth. Snow ice thickness for the flow regime including upward brine flushing is dependent on the timing of flooding, whereas for the simple flow regime it is primarily dependent only on the rate of snow accumulation.

3.4. Sensitivity to Climatic Forcing

The importance of the nature of the flooding regime is illustrated well by the response of the two models to variation in climatic forcing. Figure 7 shows results for

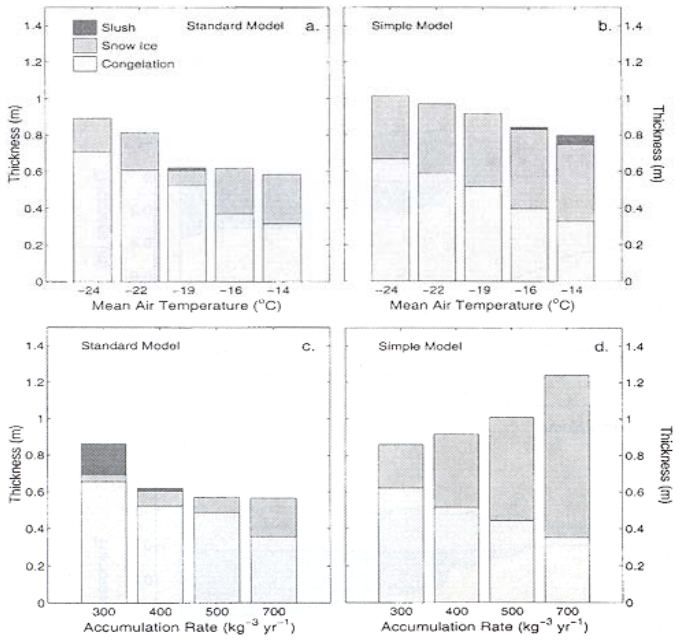

Figure 7. Dependence of modeled ice thicknesses on climatic forcing. Dependence on temperature for (a) the standard model and (b) the simple model, and dependence on accumulation rate for (c) the standard model and (d) the simple model.

both flow regimes for various climatic conditions. Simulated ice thicknesses are shown for the same growth conditions as in the previous sections, but with variations in mean temperature (Figures 7a and 7b, standard model) and in accumulation rate (Figures 7c and 7d, simple model). These variations represent the typical range of climatic conditions found in the Ross Sea, with the lower temperatures being typical winter averages observed close to the Ross Ice Shelf, and the higher temperatures being typical temperatures near the outer edge of the pack. Accumulation rates are varied between 300 and 700 kg m^{-2} yr^{-1}, the expected range for the Ross Sea [*Giovinetto et al.*, 1992].

The simple model behaves much as we might expect; increasing the mean air temperature indirectly increases the amount of snow ice formed by controlling the amount of congelation growth, with lower growth rates for higher air temperatures (Figure 7b). As the thinner ice provides less buoyancy, the accumulated snow will depress the ice surface further below sea level and therefore produce more flooding and snow ice formation. For increasing snow accumulation rates (Figure 7d) there is a fairly linear increase in snow ice thickness for the simple model. Accumulation rate has a stronger effect on snow ice thickness than does air temperature, as it more directly controls the freeboard. Congelation ice thicknesses decrease steadily with increasing accumulation rate due to bottom melting. The ice is warmed both by the insulation from the snow cover and through the transport of heat to the snow/ice interface during flooding. This leads to an increase in bottom melting rates.

The situation for the standard model is quite different (Figures 7a and 7b). As before, the amount of snow ice formed is limited by the permeability of the ice. The upward flow of brine reduces the salinity in the lower portions of the ice and results in reduced brine volumes. Once a significant amount of flushing has occurred, the brine volumes are often reduced sufficiently below the critical value for percolation that the ice remains impermeable even with substantial warming. Figure 7a reflects this, with little dependence of snow ice thickness on temperature.

There is only moderate dependence of the snow ice thickness on accumulation rate, since the ice becomes impermeable after the first or second flooding event, so there is no flooding with subsequent snowfall. The thick slush layer for the lowest accumulation rate (300 kg m^{-2} yr^{-1}) occurred at the very end of the growth period, when brine volumes increased due to warmer temperatures. This was only possible because the small degree of flushing that had occurred did not reduce salinities, and hence brine volumes, as severely as in the other cases. The dramatic differences between the simple model and the standard model show clearly the importance of brine transport processes in controlling flooding and snow ice formation.

In addition to air temperature and snow accumulation rate, ice growth and development is influenced by the oceanic heat flux. This is largely an unknown quantity, but it has been shown to have great variability in the Southern Ocean. In the Weddell Sea, winter estimates range from around 2 W m^{-2} along the continental shelf [*McPhee et al.*, 1992] to as much as 40 W m^{-2} [*Gordon and Huber*, 1990] in the eastern Weddell Sea. *Heil et al.* [1996] estimated the range to be 6-18 W m^{-2} in the east Antarctic. It has been suggested that the oceanic heat flux may be a significant controlling factor in ice development in the Ross Sea [*Jeffries and Adolphs*, 1997].

Figure 8 shows the effect of variations in ocean heat flux on both the standard and simple models. Other simulation parameters are the same as those in Figure 4. For both models the main effect is to cause an overall thinning of the total ice thickness and an increase in snow ice thickness for increasing ocean heat flux. With brine flushing included (Figures 8a and 8c) we again see low brine volumes throughout much of the ice thickness soon after substantial flooding and snow ice formation has occurred. This impermeable ice persists despite a warming of the ice with increased snow accumulation, so there is only modest dependence of snow ice thickness on ocean heat flux. Note that there is not necessarily a direct relationship between snow ice production and ocean heat flux, as less snow ice was produced in the run shown in Figure 4a, for an oceanic heat flux of 5 W m^{-2}, than for either 0 or 10 W m^{-2} (Figures 8a and 8c, respectively). The impermeable ice, however,

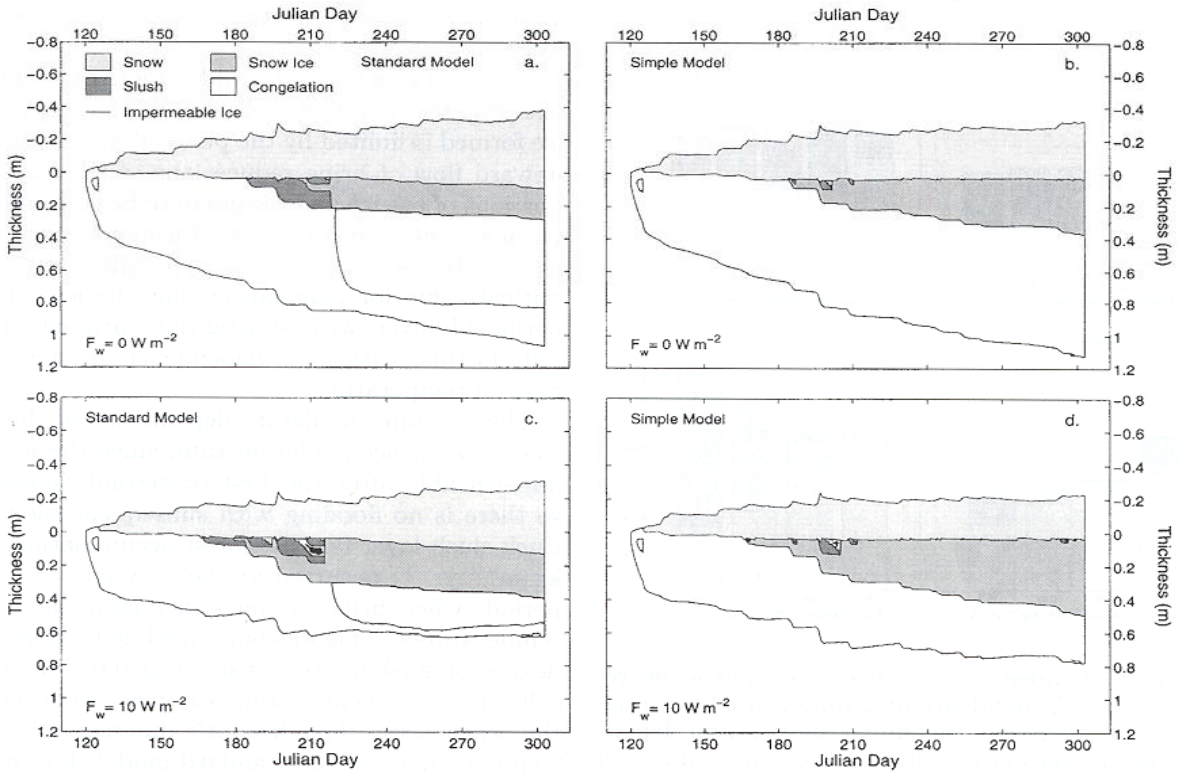

Figure 8. Ice thickness time series for variations in ocean heat flux. $F_w = 0$ W m^{-2} for (a) the standard model and (b) the simple model. $F_w = 10$ W m^{-2} for (c) the standard model and (d) the simple model. In Figure 4, $F_w = 5$ W m^{-2}.

allows a thick snow cover to develop without flooding. This insulates the ice and permits significant ablation from the base for the case of a high oceanic heat flux (Figure 8c).

Without brine flushing (Figures 8b and 8d), the main effect of the higher ocean heat flux is to slow congelation ice growth and even to promote basal melting. This amplifies the snow load, permitting increased flooding and snow ice development.

3.5. Effects of Brine Flow Regime

As the conditions necessary for flow exhibit a critical behavior, in that the brine volume must be above a threshold value for flooding to occur, subtle influences on brine volume may have quite substantial effects. Variations in the nature of brine transport are quite important in controlling the mass balance, as shown above by the profound effects of brine flushing. However, the precise nature of this brine percolation, if indeed it even takes place, is largely unknown. For example, Figure 3 shows that the permeability of sea ice is not a well-defined quantity. Figure 9 shows the effects of variations in ice permeability, for three different dates of initial ice formation. Final ice thicknesses are shown for three regimes: the standard permeability, K, defined by the fit to the data from Figure 3, and a low- and a high-permeability regime, assigned permeabilities of $0.1K$ and $10K$, respectively, for the same brine volumes. Other parameters are the same as the simulation shown in Figure 4a. Contrary to what we might expect, there is a decrease in the amount of snow ice formed using the higher permeability. Flooding and refreezing tends to occur in one major event, typically lasting several hours to a day, after which brine volumes in the lower portions of the ice are greatly reduced, usually rendering the ice impermeable for the remainder of the growth season. In this case the ice is permeable enough that the duration of the flooding event is governed by the rate of snow accumulation. In the case of low permeability, the flow velocity is so slow that the flooding is sustained over a period many days, so that subsequent snow accumulation causes flooding events to overlap one another, and a continuous slow percolation of brine occurs. This provides a continual flux of heat to the ice and the slush, delaying the freezing of the flooded layer and thereby keeping the ice permeable. This sustained flooding increases the upward flushing of the brine network, so that despite the warming provided by the brine flow, enough salt is eventually flushed from the ice to reduce brine volumes below the percolation threshold. This prevents any further drainage of salt from the slushy layer, so it becomes much more difficult to freeze. As a result, in all three simulations shown in Figure 9 for the low-permeability case, the flooded layer never completely freezes, even though it generally exists for 90 days or more. In the

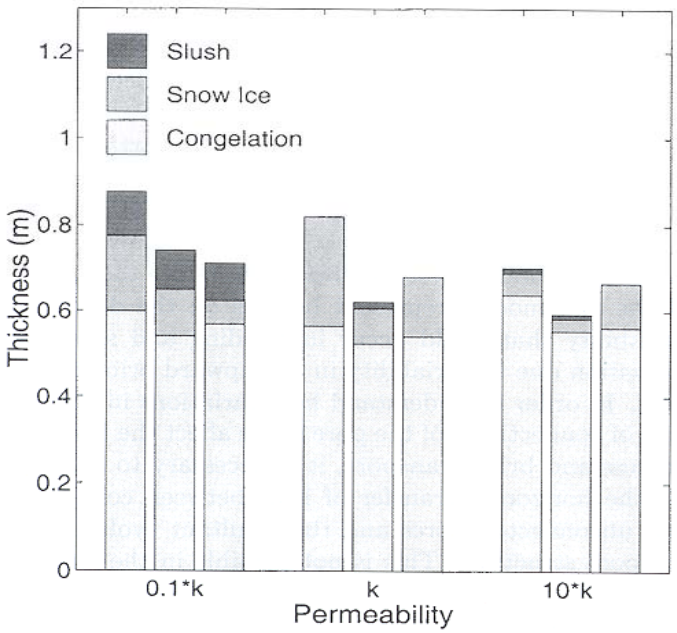

Figure 9. Thicknesses of congelation ice, snow ice, and slush for the standard model for variations in ice permeability. Standard permeability, K, is given by the fit in Figure 3. The high-permeability plot represents a tenfold increase in permeability; the low-permeability represents a tenfold decrease in permeability. Results for each permeability are shown for three different dates of initial ice formation (from left to right, Julian days 91, 121, and 151).

simulations using the higher permeability, flooding and subsequent refreezing is relatively rapid (typically a few days). This allows temperature gradients to reestablish quickly after flooding, reducing brine volumes to below the percolation threshold. Hence we see very little snow ice formed in this regime.

It is evident that the nature of the processes involved in brine transport are vital in controlling both the timing and magnitude of flooding and snow ice formation. At this point, it would be prudent to examine the assumptions used in formulating the standard model. To this end we examine the effects of the convective exchange of brine during the freezing of the flooded layer. In Figure 10 we examine two cases: (1) Heat flux due to convective overturn of brine from the flooded layer to the ocean below is neglected, which permits temperature gradients to propagate through the ice when a flooded layer is present (equivalent to treating the brine in the flooded layer in the same way thermodynamically as liquid inclusions in the ice below); and (2) salt drained from the slush is redistributed evenly among the ice layers below during freeze-up. This provides an estimate of the effects of possible salination of the ice from salt redistribution in maintaining ice permeability and allows an assessment of the effect of the limitations of equation (11) on the results.

Results are shown in Figure 10 for three different regimes: excluding convection (Figure 10a), including salt redistribution (Figure 10b), and the standard model (Figure 10c). Without convection, upward flushing of brine during flooding is very effective, so that the ice becomes impermeable once the thermal gradient is reestablished. This leaves a thin, saline (30-40‰) slush at the base of the snow cover that cannot freeze without drainage of brine or a severe drop in air temperatures. As a result, without convection of brine, the standard model will rarely produce any snow ice at all. With salt redistribution included, the salt transferred from the slush layer to the ice increases the ice salinity somewhat, maintaining the porosity above the percolation threshold longer than for the standard model, allowing increased flooding. However, brine flushing is still a very effective process in reducing the ice salinity, so that the ice still becomes impermeable, and only a moderate increase in snow ice production occurs.

4. Discussion

Flooding and snow ice formation are seen to be critically dependent on a number of factors. In particular, the nature of the flow process which brings brine and seawater to the surface during a flooding event is crucial in determining both the mass balance of the ice and its physical properties. Permitting interaction of the flooding brine with the porous ice matrix produces

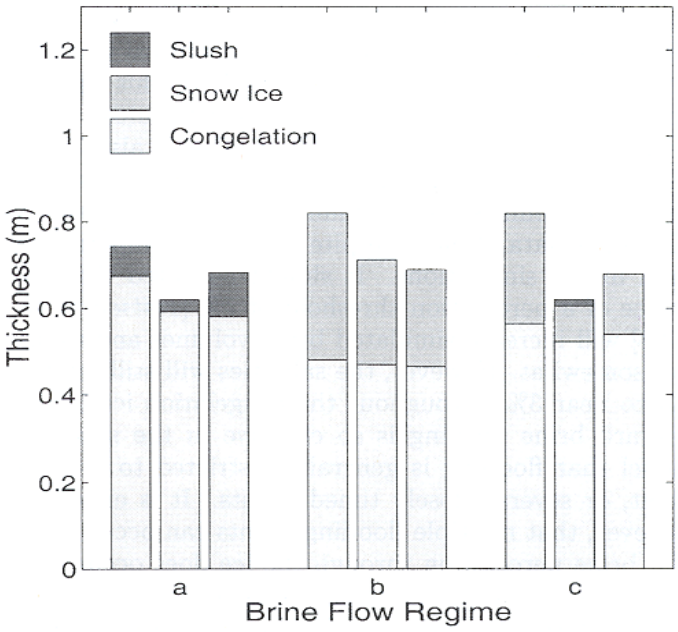

Figure 10. Thicknesses of congelation ice, snow ice, and slush at the end of the simulation period for different parameterizations of the brine exchange between the slush and underlying ice: no convection between slush and ice (bars marked "a"), redistribution of brine drained from slush to the ice (bars marked "b"), and standard model (bars marked "c"). Results for each case are shown for three different dates of initial ice formation (from left to right, Julian days 91, 121, and 151).

drastically different results than simple flooding of the surface with seawater in terms of amounts of snow ice formed, and in turn, the thickness of the remaining snow cover, and in terms of the salinity and porosity (brine volume) structure of the ice. Upward brine flushing during flooding reduces ice porosity to such a degree that it generally restricts flooding to one major event or a series of closely spaced events. This typically restricts snow ice thicknesses to less than 20 cm. The overall mass balance is then controlled primarily by climatic factors early in ice development. As flooding and snow ice formation are dependent on a critical percolation threshold, the nature of the physical processes involved is as important as climatic effects in determining quantities of snow ice produced. With the simple model, brine volumes remained consistently above the percolation threshold, so snow ice thicknesses were primarily dependent on snow load, and the overall ice thickness was much less dependent on early growth conditions.

As presented, upward percolation of brine by uniform Darcian flow through a porous ice matrix seems an unlikely candidate to be responsible for the bulk of the flooding process. Resultant snow ice thicknesses appear to be significantly lower than expected, and highly negative freeboards (as much as -20 cm) persist throughout much of the growth season, in conflict with observations (Figure 1). Large negative freeboards are generally associated with deformational features, and not level ice. Furthermore, the very low salinities that result from this upward flushing of brine are not consistent with observations. Brine volumes below the critical value for permeable ice are a ubiquitous result of this upward brine flushing and are typically present for most of the growth period after initial flooding. This is also inconsistent with observations, which show that most sea ice has brine volumes greater than 5% (M. O. Jeffries, unpublished data, 1995), despite lower ice temperatures than in the simulations. It should be noted that the choice of a percolation threshold of 7% [*Fritsen et al.*, 1998] will increase simulated brine volumes and salinities somewhat. However, the salinities will still tend to fall to near 3‰ throughout the congelation ice layers. Upward brine flushing is so effective in the standard model that flooding is generally restricted to a single event, or several closely timed events. It is expected, however, that multiple flooding events can occur.

If brine percolation through the ice does occur with any frequency in the Antarctic pack, it is undoubtedly not a uniform phenomenon. Horizontal inhomogeneities in the salinity and pore structure of the ice sheet will likely cause large spatial variations in the flow, so that only some areas of the ice sheet are affected internally by the flooding. If the permeable region is restricted spatially, or if the permeability is high enough in a given area, the flow may be sufficiently rapid that the assumption of local thermal equilibrium is not met. In this case the thermal response of the ice is reduced, and substantial flow may occur without the pathways freezing shut due to the brine transport. Modeling of the flow then becomes very difficult, since detailed knowledge of the porosity structure of the ice is required to account for both the flow and heat transfer, and the heat transfer relations become quite complicated. Furthermore, it may be necessary to account for horizontal transport of the flooding brine through the snow. Note that the extreme case of localized flow is roughly equivalent to the simple model presented here. Therefore the results of the two models represent bounds on the degree of variability that could occur in flooding and snow ice formation due to variability in the upward brine transport. In order to understand how variations in the degree of connectivity of the pore space affect the flooding process and brine transport, it is necessary to account for the horizontal transfer of heat between connected and unconnected pores and the resultant evolution of the pore structure. This is not possible in the current model. It will be addressed in a subsequent version.

A significant area of weakness in the models is the treatment of brine drainage and convection in the ice. At present, the only parameterizations available to account for gravity drainage are those of *Cox and Weeks* [1975], which were derived for laboratory-grown NaCl congelation ice. Growth conditions are quite different for the modeled sea ice. First, the ice is generally warmer than that in the Cox and Weeks experiments, with temperature gradients generally lower than those measured in the laboratory. Second, model salinity profiles are "top heavy" after flooding, especially in the standard model, with very high salinities in the upper portions of the ice sheet (15-25‰), and very low, near-uniform values in the lower ice (~2.5‰ for the standard model, 3-5‰ for the simple model). It seems likely that brine drainage from the upper ice will have an impact on the salinity of the lower ice as it drains through the ice sheet [*Kovacs*, 1996]. Third, the very high porosities of the slush and snow ice layer could lead to brine pockets large enough for internal convection to permit them to migrate very quickly, possibly leading to significant resalination of the lower, low-salinity ice layers. Finally, convection of brine during freeze-up of the flooded layer will likely transport salt from the upper ice to that below. Observations indicate that brine convection may be quite important in brine transport for flooded ice [*Lytle and Ackley*, 1996], and may represent a significant redistribution of salt [*Hudier et al.*, 1995]. A simple parameterization of salt redistribution showed that while this process can increase the porosity of the ice temporarily, brine flushing during flooding is still the controlling process on the ice permeability. While it is possible that this simple approach underestimates the salt redistribution, recent results with a two dimensional convective model indicate that this effect may be small [*Maksym and Jeffries*, 2000]. It has been demonstrated that the salinity characteristics may play a crucial role in controlling the ice mass balance through the flooding and snow ice formation process; a proper

treatment of brine transport in sea ice is essential to understanding the role of this process in Antarctic sea ice development.

It was noted above that the ice in the simulations was markedly warmer than is typically observed. While this is in part due to fairly thin ice and thick snow cover, this cannot account for all of the difference. We attribute this partly to the low snow thermal conductivity given by (8). While we do not believe that this gives unrepresentative values, it may not account for all of the heat transfer through the snow. Enhanced vapor transport within warm snow may increase the effective thermal conductivity somewhat. Wind pumping and snow redistribution effects may cool the snow. As temperature gradients within the snow were very large, convection may have also played a role, although the presence of numerous icy layers [*Sturm et al.*, 1998] would seem to preclude this. Recent observations in the Arctic indicate that large lateral variations in snow depth may cause a focussing effect on the heat flow and may have a substantial effect on the thermal regime of sea ice (M. Sturm, personal communication, 2000).

The inclusion of depth hoar could have an important effect on the results due to its very low thermal conductivity. However, this would raise the ice temperatures even further. While this could render the ice permeable for a longer period, brine flushing would then remove even more salt from the lower ice layers, increasing the disparity between simulation results and field data.

5. Conclusions

A one-dimensional sea ice growth model has been developed to investigate the factors controlling flooding and snow ice formation. The flooding process is modeled by two methods. In the first, dubbed the standard model, flooding is modeled by brine percolation upward through the porous ice. In the second, or simple model, seawater is assumed to infiltrate into the snow through isolated areas, such as large drainage tubes or cracks, and does not displace the brine entrapped in the bulk ice. Results indicate that the evolution and mass balance of the ice are very dependent on the physical process by which flooding takes place.

The simple model produces the most reasonable results. Congelation and snow ice thicknesses are realistic, and salinities in both the snow ice and congelation ice layers compare reasonably well with field data. The standard model, on the other hand, produces little snow ice despite highly negative freeboards. Salinities within the congelation ice become unrealistically low as a result of upward brine flushing, creating very low brine volumes and rendering much of the ice impermeable, even though ice temperatures are high.

The most important factor in controlling the ice mass balance is the presence of a snow cover. Initial congelation ice growth is generally very rapid, but once a significant amount of snow has accumulated, further thickening by congelation ice growth is greatly inhibited, or there may even be bottom melting. The thickness of congelation ice late in the growth season is very strongly dependent on the oceanic heat flux. Subsequent ice growth is primarily through flooding and snow ice formation for both models. Since the standard model generally produces little snow ice, the total ice thickness is highly dependent on climatic conditions early in ice development. This makes the ice thickness somewhat unpredictable as it is nearly independent of its age. For the simple model, while congelation ice thickness is also dependent on early growth conditions, snow ice thickness is a strong function of snow load, so that the total ice thickness is much more predictable, and ice thickness generally increases with age.

The models presented here, while inappropriate for use in predicting ice mass balance and salinity characteristics, illustrate the importance of the various factors controlling flooding and snow ice formation, and demonstrate the need for improved understanding of the brine transport processes in sea ice in order to understand not only the salinity structure of the ice, but also the ice mass balance. The actual brine flow regime likely lies somewhere between the two models. If brine percolation through the bulk of the ice is a major component of the flooding process, then either significant convection and redistribution of brine must be occurring to maintain the ice permeability, or upward brine flushing is spatially nonuniform. Either the process is restricted to areas of high ice permeability, such as in large drainage tubes or fractures, or local variations in pore geometry and thermal transport are significant in modifying the salt transport in individual pores.

Acknowledgments. This research was funded by NSF grant OPP 9316767. We would like to thank the NOAA-CIRES Climate Diagnostics Center for providing the NCEP reanalysis data. Temperature data for Possession Island were provided by the University of Wisconsin AWS project. This work was supported in part by a grant of HPC time from the Arctic Region Supercomputing Center. Thanks are due to H. Eicken, W. F. Weeks, and three anonymous reviewers for their valuable comments on an earlier version of this paper.

References

Abel's, G., Beobachtungen der täglichen Periode der Temperatur im Schnee und Bestimmung des Wärmeleitungsvermogens des Schnees als Function seiner Dichtigkeit (Observations of daily temperature variations in a snow cover), *Rep. Meteorol. Herausgegeben K. Akad. Wiss.*, *15*, 1–53, 1893.

Ackley, S. F., Sea-ice pressure ridge microbial communities, *Antarct. J. U.S.*, *21*(5), 172–174, 1986.

Ackley, S. F., and C. W. Sullivan, Physical controls on the development and characteristics of Antarctic sea ice biological communities - A review and synthesis, *Deep Sea Res.*, *41*, 1583–1604, 1994.

Adolphs, U., Ice thickness variability, isostatic balance and potential for snow ice formation on ice floes in the south

polar Pacific Ocean, *J. Geophys. Res.*, *103*, 24,675–24,691, 1998.

Allison, I., R. E. Brandt, and S. G. Warren, East Antarctic sea ice: Albedo, thickness distribution, and snow cover, *J. Geophys. Res.*, *98*, 12,417–12,429, 1993.

Anderson, E. A., A point energy and mass balance model of a snow cover, *NOAA Tech. Rep. NWS 19*, 150 pp., U.S. Dep. of Commer., Washington, D.C., 1976.

Arons, E. M., and S. C. Colbeck, Geometry of heat and mass transfer in dry snow: A review of theory and experiment, *Rev. Geophys.*, *33*, 463–493, 1995.

Bear, J., *Dynamics of Fluids in Porous Media*, Elsevier Sci., New York, 1972.

Bennington, K. O., Some crystal growth features of sea ice, *J. Glaciol.*, *4*, 669–688, 1963.

Bennington, K. O., Desalination features in natural sea ice, *J. Glaciol.*, *6*, 845–857, 1967.

Choudhury, B., Radiative properties of snow for clear sky solar radiation, *Cold Reg. Sci. Technol.*, *4*, 103–120, 1981.

Colbeck, S. C., Ice crystal morphology and growth rates at low supersaturations and high temperatures, *J. Appl. Phys.*, *54(*5), 2677–2682, 1983.

Cole, D. M., and L. H. Shapiro, Observations of brine drainage networks and microstructure of first-year sea ice, *J. Geophys. Res.*, *103*, 21,739–21,750, 1998.

Cox, G. F. N., and W. F. Weeks, Brine drainage and initial salt entrapment in sodium chloride ice, *CRREL Res. Rep. 345*, 46 pp., U.S. Army Cold Reg. Res. and Eng. Lab., Hanover, N.H., 1975.

Cox, G. F. N., and W. F. Weeks, Numerical simulations of the profile properties of undeformed first-year sea ice during the growth season, *J. Geophys. Res.*, *93*, 12,449–12,460, 1988.

Crocker, G. B., and P. Wadhams, Modelling Antarctic fast-ice growth, *J. Glaciol.*, *35*, 3–8, 1989.

Eicken, H., Salinity profiles of Antarctic sea ice: Field data and model results, *J. Geophys. Res.*, *97*, 15,545–15,557, 1992.

Eicken, H., M. Lange, H.-W. Hubberten, and P. Wadhams, Characteristics and distribution patterns of snow and meteoric ice in the Weddell Sea and their contribution to the mass balance of sea ice, *Ann. Geophys.*, *12*, 80–93, 1994.

Eicken, H., H. Fischer, and P. Lemke, Effects of the snow cover on Antarctic sea ice and potential modulation of its response to climate change, *Ann. Glaciol.*, *21*, 369–376, 1995.

Fritsen, C. H., S. F. Ackley, J. N. Kremer, and C. W. Sullivan, Flood-freeze cycles and microalgal dynamics in Antarctic pack ice, in *Antarctic Sea Ice: Biological Processes, Interactions and Variability*, edited by M. P. Lizotte and K. O. Arrigo, *Antarct. Res. Ser.*, vol. 73, pp. 1–21, AGU, Washington, D.C., 1998.

Giovinetto, M. B., D. Bromwich, and G. Wendler, Atmospheric net transport of water vapor and latent heat across 70°S, *J. Geophys. Res.*, *97*, 917–930, 1992.

Golden, K. M., S. F. Ackley, and V. I. Lytle, The percolation phase transition in sea ice, *Science*, *282*, 2238–2241, 1998.

Goodrich, L. E., Efficient numerical technique for one-dimensional thermal problems with phase change, *Int. J. Heat Mass Transfer*, *21*, 615–621, 1978.

Gordon, A. L., and B. A. Huber, Southern Ocean winter mixed layer, *J. Geophys. Res.*, *95*, 11,655–11,672, 1990.

Grenfell, T. C., The effects of ice thickness on the exchange of solar radiation over the polar oceans, *J. Glaciol.*, *22*, 305–320, 1979.

Heil, P., I. Allison, and V. Lytle, Seasonal and interannual variations of the oceanic heat flux, *J. Geophys. Res.*, *101*, 25,741–25,752, 1996.

Hill, J. M., *One-Dimensional Stefan Problems: An Introduction*, *Pitman Monogr. Surv. Pure Appl. Math.*, vol. 31, John Wiley, New York, 1987.

Hudier, E. J.-J., R. Ingram, and K. Shirasawa, Upward flushing of sea water through first year ice, *Atmos. Ocean*, *33*, 569–580, 1995.

Jeffries, M. O., and U. Adolphs, Early winter ice and snow thickness distribution, ice structure and development of the western Ross Sea pack ice between the ice edge and the Ross Ice Shelf, *Antarct. Sci.*, *9*, 188–299, 1997.

Jeffries, M. O., A. Worby, K. Morris, and W. Weeks, Seasonal variations in the properties and structural composition of sea ice and snow cover in the Bellingshausen and Amundsen Seas, Antarctica, *J. Glaciol.*, *43*, 138–152, 1997.

Jeffries, M. O., B. Hurst-Cushing, H. R. Krouse, and T. Maksym, The role of snow in the thickening and mass budget of first-year floes in the eastern Pacific sector of the Antarctic pack ice, *Geophys. Inst. Rep. UAGR-327*, 34 pp., Univ. of Alaska Fairbanks, 1998a.

Jeffries, M. O., S. Li, R. A. Jaña, H. R. Krouse, and B. Hurst-Cushing, Late winter first-year ice floe thickness variability, seawater flooding and snow ice formation in the Amundsen and Ross Seas, in *Antarctic Sea Ice: Physical Processes, Interactions and Variability*, edited by M. O. Jeffries, *Antarct. Res. Ser.*, vol. 74, pp. 69–87, AGU, Washington, D.C., 1998b.

Key, J. R., R. Silcox, and R. Stone, Evaluation of surface radiative flux parameterizations for use in sea ice models, *J. Geophys. Res.*, *101*, 3839–3849, 1996.

Kovacs, A., Sea ice part I. Bulk salinity versus ice floe thickness, *CRREL Rep. 96-7*, 16 pp., U.S. Army Cold Reg. Res. and Eng. Lab., Hanover, N.H., 1996.

Kuroiwa, D., Liquid permeability of snow, *IAHS Publ.*, *79*, 380–391, 1968.

Lake, R. A., and E. L. Lewis, Salt rejection by sea ice during growth, *J. Geophys. Res.*, *75*, 583–597, 1970.

Lange, M. A., S. F. Ackley, P. Wadhams, G. S. Dieckmann, and H. Eicken, Development of sea ice in the Weddell Sea, *Ann. Glaciol.*, *12*, 92–96, 1989.

Lange, M. A., P. Schlosser, S. F. Ackley, P. Wadhams, and G. Dieckmann, $\delta^{18}O$ concentrations in sea ice of the Weddell Sea, *J. Glaciol.*, *36*, 315–323, 1990.

Leppäranta, M., A growth model for black ice, snow ice and snow thickness in subarctic basins, *Nord. Hydrol.*, *14*, 59–70, 1983.

Lytle, V. I., and S. F. Ackley, Heat flux through sea ice in the western Weddell Sea: Convective and conductive transfer processes, *J. Geophys. Res.*, *101*, 8853– 8868, 1996.

Maksym, T., and M. O. Jeffries, Bulk salinity characteristics of first-year sea ice in the Pacific sector of the southern oceans, *Antarct. J. U.S.*, *31(*2), 99–101, 1996.

Maksym, T., and M. O. Jeffries, Phase and compositional evolution of the flooded layer during snow ice formation on Antarctic sea ice, *Ann. Glaciol.*, in press, 2001.

Massom, R. A., M. R. Drinkwater, and C. Haas, Winter snow cover on sea ice in the Weddell Sea, *J. Geophys. Res.*, *102*, 1101–1117, 1997.

Maykut, G. A., Energy exchange over young sea ice in the central Arctic, *J. Geophys. Res.*, *83*, 3646–3658, 1978.

Maykut, G. A., and N. Untersteiner, Some results from a time-dependent thermodynamic model of sea ice, *J. Geophys. Res.*, *76*, 1550–1576, 1971.

McGuinness, M. J., H. J. Trohdahl, K. Collins, and T. G. Haskell, Non-linear thermal transport and brine convection in first-year sea ice, *Ann. Glaciol.*, *27*, 471–476, 1998.

McPhee, M. G., D. G. Martinson, and J. H. Morison, Upper-ocean measurements of turbulent flux in the western Weddell Sea, *Antarct. J. U.S.*, *27(*5), 103–105, 1992.

Niedrauer, T. M., and S. Martin, An experimental study of

brine drainage and convection in young sea ice, *J. Geophys. Res.*, *84*, 1176–1186, 1979.

Ono, N., and T. Kasai, Surface layer salinity of young sea ice, *Ann. Glaciol.*, *6*, 298–299, 1985.

Patankar, S. V., *Numerical Heat Transfer and Fluid Flow*, Hemisphere, New York, 1980.

Perovich, D. K., and A. J. Gow, A quantitative description of sea ice inclusions, *J. Geophys. Res.*, *101*, 18,327–18,343, 1996.

Saeki, H., T. Takeuchi, M. Sakai, and E. Suenaga, Experimental study on permeability coefficient of sea ice, in *Ice Technology, Proceedings: 1st International Conference*, edited by T. K. S. Murthy, J. J. Connor, and C. A. Brebbia, pp. 237–246, Springer-Verlag, New York, 1986.

Saito, T., and N. Ono, Percolation in sea ice, I, Measurements of kerosene permeability of NaCl ice, *Low Temp. Sci., Ser. A*, *37*, 55–62, 1978.

Schwerdtfeger, P., The thermal properties of sea ice, *J. Glaciol.*, *4*, 789–807, 1963.

Sturm, M., The role of thermal convection in heat and mass transport in the subarctic snow cover, *CRREL Rep. 91-19*, 82 pp., U.S. Army Cold Reg. Res. and Eng. Lab., Hanover, N.H., 1991.

Sturm, M., J. Holmgren, M. Konig, and K. Morris, The thermal conductivity of seasonal snow, *J. Glaciol.*, *43*, 26–41, 1997.

Sturm, M., K. Morris, and R. Massom, The winter snow cover of the west Antarctic pack ice: Its spatial and temporal variability, in *Antarctic Sea Ice: Physical Processes, Interactions and Variability*, edited by M. O. Jeffries, *Antarctic Research Series*, vol. 74, pp. 1–18, AGU, Washington, D.C., 1998.

Wade, R. H., Studies of the geophysics of sea ice, Ph.D. thesis, Univ. of Alaska Fairbanks, 1993.

Weeks, W. F., and S. F. Ackley, The growth, structure and properties of sea ice, in *Geophysics of Sea Ice*, edited by N. Untersteiner, *NATO ASI Ser., Ser. 3*, vol. 146, pp. 9–146, Plenum, New York, 1986.

Weissenberger, J., G. Dieckmann, R. Gradinger, and M. Spindler, Sea ice: A cast technique to examine and analyze brine pockets and channel structure, *Limnol. Oceanogr.*, *37*, 179–183, 1992.

Weller, G., Radiation flux investigation, *AIDJEX Bull.*, *14*, 28–30, 1972.

Wooding, R. A., The stability of a viscous liquid in a vertical tube containing porous material, *Proc. R. Soc. London, Ser. A*, *252*, 120–134, 1959.

Worby, A. P., M. O. Jeffries, W. F. Weeks, K. Morris, and R. Jaña, The thickness distribution of sea ice and snow cover during late winter in the Bellingshausen and Amundsen Seas, Antarctica, *J. Geophys. Res.*, *101*, 28,441–28,455, 1996.

Worby, A. P., R. A. Massom, I. Allison, V. I. Lytle, and P. Heil, East Antarctic sea ice: A review of its structure, properties, and drift, in *Antarctic Sea Ice: Physical Processes, Interactions and Variability*, edited by M. O. Jeffries, *Antarctic Research Series*, vol. 74, pp. 41–67, AGU, Washington, D.C., 1998.

Worster, M. G., Solidification of an alloy from a cooled boundary, *J. Fluid Mech.*, *167*, 481–501, 1986.

Yen, Y.-C., Review of thermal properties of snow, ice and sea ice, *CRREL Rep. 81-10*, 27 pp., U.S. Army Cold Reg. Res. and Eng. Lab., Hanover, N.H., 1981.

Zillman, J. W., A study of some aspects of the radiation and heat budgets of the Southern Hemisphere oceans, *Meteorol. Stud. 26*, 562 pp., Bur. of Meteorol., Dep. of the Inter., Canberra, A.C.T., Australia, 1972.

M. O. Jeffries and T. Maksym, Geophysical Institute, University of Alaska Fairbanks, 903 Koyukuk Drive, Box 757320, Fairbanks, AK, 99775-7320. (maksym@arsc.edu)

(Received February 22, 1999; revised July 6, 2000; accepted July 14, 2000.)